# A Novel Approach to Design Low-Cost Two-Stage Frequency-Response Masking Filters

Ying Wei, *Member, IEEE*, Shaoguang Huang, and Xiaojie Ma

***Abstract*—The multistage frequency-response masking (FRM) technique is widely used to reduce the complexity of a filter when the transition bandwidth is extremely small. In this brief, a real generalized two-stage FRM filter without any constraint on the subfilters or the interpolation factors was proposed. New principles and equations were deduced to determine the design parameters. The subfilters were then jointly optimized using nonlinear optimization. Experiential results show that when the proposed algorithm obtains different solutions with the conventional algorithm, the solution of the proposed approach is better with less number of filter coefficients and sometimes with lower delay as well than the conventional two-stage FRM, which can lead to a reduced hardware cost in applications.**

***Index Terms*—Finite-impulse response filters, frequency-response masking (FRM), narrow transition-band filters, optimization.**

## I. Introduction

The frequency-response masking (FRM) technique is an efficient method for the design of the finite-impulse response filters with very narrow transition bands [1], [2]. The overall transfer function $H(z)$ is given by (1), where $M$ is an interpolation factor of the prototype filter $H_a(z)$. In order to remove the redundant periodic bands, two masking filters $H_{ma}(z)$ and $H_{mc}(z)$ are employed. In a case where the transition bandwidth is extremely narrow, to further reduce the complexity, multistage FRM is used. The transfer function $H(z)$ of an $R$-stage FRM filter is shown in equation (2)

$$H(z)=H_a(z^M)H_{ma}(z)+\left(z^{-\frac{M(N_a-1)}{2}}-H_a(z^M)\right)H_{mc}(z) \quad (1)$$

$$H_a^{(i-1)}(z)=H_a^{(i)}(z^{M_i})H_{ma}^{(i)}(z)+H_c^{(i)}(z^{M_i})H_{mc}^{(i)}(z) \quad (2)$$

where $i=1,\ldots,R$. $M_i$ is the interpolation factor in the $i$th stage. $H_a^{(i)}(z)$ is the prototype filter in the $i$th stage. $H_c^{(i)}(z^{M_i})$ is the complement of $H_a^{(i)}(z^{M_i})$. $H_{ma}^{(i)}(z)$ and $H_{mc}^{(i)}(z)$ are the masking filters of the $i$th stage. The overall filter is $H_a^{(0)}(z)$.

Manuscript received January 17, 2015; revised April 7, 2015; accepted June 12, 2015. Date of publication July 17, 2015; date of current version September 25, 2015. This work was supported in part by the Fundamental Research Funds of Shandong University under Grant 2015CJ029, by the Specialized Research Fund for the Doctoral Program of Higher Education of China under Grant 20120131120088, by Shandong Province Science and Technology Development Plan under Grant 2013GGX10103, by the Promotive Research Foundation for Excellent Young and Middle-Aged Scientists of Shandong Province under Grant BS2013DX042, and by Taishan Scholar Foundation Project under Grant 1170082963013. This brief was recommended by Associate Editor G. J. Dolecek.

Y. Wei and S. Huang are with the School of Information Science and Engineering, Shandong University, Jinan 250100, China (e-mail: eleweiy@sdu.edu.cn).

X. Ma is with Qilu Hospital of Shandong University, Jinan 250012, China.

Digital Object Identifier 10.1109/TCSII.2015.2457794

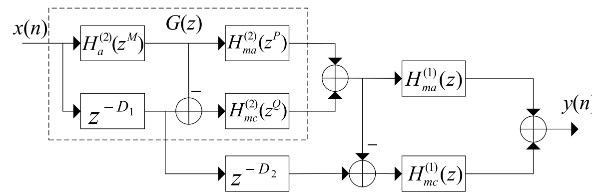


Fig. 1. Two-stage FRM approach.

In this brief, we focus on the most commonly used multistage FRM, i.e., the two-stage FRM.

The structure of a two-stage FRM filter is shown in Fig. 1. The band-edge-shaping filter is denoted as $G(z)$. For conventional two-stage FRM, based on (2), we can see that $P=Q$, and there is a constraint among the interpolation factors, i.e.,

$$M=kP=kQ, \quad k \text{ is a positive integer.} \quad (3)$$

There were many improvements that addressed the multistage FRM. In [3], a joint optimization of the subfilters was proposed. It consists of a sequence of linear updates for the design variables. Each update is based on the semidefinite programming. Moreover, the group delay of the overall filter was reduced by using the nonlinear-phase prototype filter. In [4], an iterative algorithm combining linear programming was proposed. The subfilters in the second stage were first updated iteratively until meeting the prescribed tolerance, and then, the subfilters in the first stage were updated similarly. It achieved 25% savings in terms of the number of multipliers compared with the original method. The design of the multistage FRM filter was converted into the weighted least-squares problem in [5], which led to a satisfactory savings in the effective filter length. A neural network algorithm was proposed to optimize the subfilters in [6] and achieved better performance both in passband ripples and stopband attenuation than several existing methods. In [7] and [8], a two-step design technique was improved. An initial solution was first provided by a simple design method. Then, a suboptimal solution would be found with the aid of a nonlinear optimization algorithm. The complexity of multistage FRM filters using the proposed method in [7] accounted for 70% of that using original FRM design methods.

The aforementioned improvements are under the assumption of (3). The question is "Are the constraints necessary?" For the two-stage FRM, the direct result of (3) is that the output of the second stage produces a periodic magnitude response. However, as long as the second stage can provide the transition band of the overall filter, the output of it can be "periodic" or "nonperiodic." Based on this understanding, we proposed an FRM structure with a nonperiodic band-edge-shaping filter in [9]. The constraints on the interpolation factors were removed. However, a constraint on the subfilters that all the subfilters in

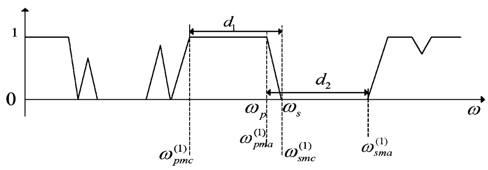


Fig. 2. Possible magnitude response of $G(z)$.

the second stage must come from the same prototype filter was added to facilitate the design. In this brief, we further removed the constraint on the subfilters to obtain a real generalized two-stage structure. In fact, the structure in [9] can be viewed as the specialized case of the proposed structure here. Based on the generalized two-stage FRM structure, new principles and equations were deduced to determine the specifications of the five different subfilters. Furthermore, a two-step nonlinear optimization technique [8] was used to jointly optimize the subfilters.

This brief is organized as follows. In Section II, the proposed structure is described in detail. The determination of the design parameters for the proposed structure is discussed. In Section III, design examples are presented to illustrate the efficiency in the complexity and the group delay.

## II. Proposed Generalized Two-Stage FRM Filter

In the proposed two-stage FRM structure shown in Fig. 1, $M$, $P$, and $Q$ are free parameters. The transfer function $H(z)$ of the overall filter is produced by

$$H(z) = G(z)H^{(1)}_{ma}(z) + \left(z^{-(D_1+D_2)} - G(z)\right) H^{(1)}_{mc}(z). \quad (4)$$

The $z$-transform transfer function of $G(z)$ is represented by

$$G(z) = H^{(2)}_a(z^M)F^{(2)}_1(z) + \left(z^{-D_1} - H^{(2)}_a(z^M)\right) F^{(2)}_2(z) \quad (5)$$

where $F^{(2)}_1(z)$ and $F^{(2)}_2(z)$ are the masking filters of the second stage, i.e.,

$$F^{(2)}_1(z) = \begin{cases} H^{(2)}_{ma}(z^P) & \text{case}_P = A \\ \text{the complement of } H^{(2)}_{ma}(z^P) & \text{case}_P = B \end{cases}$$
$$F^{(2)}_2(z) = \begin{cases} H^{(2)}_{mc}(z^Q) & \text{case}_Q = A \\ \text{the complement of } H^{(2)}_{mc}(z^Q) & \text{case}_Q = B. \end{cases}$$

The transition band of the overall filter can be formed by $H^{(2)}_a(z^M)$ (Case $A$) or its complement (Case $B$). Moreover, the masking for the upper branch of Fig. 1 can be done by $H^{(2)}_{ma}(z^P)$ (Case$_p = A$) or its complement (Case$_p = B$). The masking for the lower branch of Fig. 1 can be done by $H^{(2)}_{mc}(z^Q)$ (Case$_q = A$) or its complement (Case$_q = B$).

The possible magnitude response is shown in Fig. 2, where $\omega_p$ and $\omega_s$ represent the passband edge and the stopband edge of the overall filter, respectively. It should be noted that this magnitude response may not be periodic since there is no constraint among $M$, $P$, and $Q$. The band edges of $H^{(1)}_{ma}(z)$, $\omega^{(1)}_{pma}$, and $\omega^{(1)}_{sma}$ and the band edges of $H^{(1)}_{mc}(z)$, $\omega^{(1)}_{pmc}$, and $\omega^{(1)}_{smc}$ are also shown in the figure. We denote the distance between $\omega^{(1)}_{pmc}$ and $\omega^{(1)}_{smc}$ by $d_1$ and the distance between $\omega^{(1)}_{pma}$ and $\omega^{(1)}_{sma}$ by $d_2$. The pass- and stopband ripples of the overall filter are denoted by $\delta_p$ and $\delta_s$, respectively. Since the conventional way

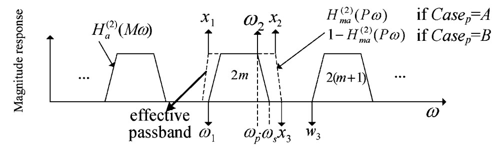


Fig. 3. Magnitude response of the upper branch of $G(z)$.

to determine the band edges of the subfilters cannot be used any more, new design method needs to be developed.

The proposed structure contains several alternatives depending on the location of band edges. The set of $[M, P, Q]$ that leads to the lowest complexity in terms of the number of multipliers is obtained by global search. For a given $M$, $P$, and $Q$, let us illustrate how the parameters of these subfilters are determined.

The determination of the band edges of $H^{(2)}_a(z)$ follows the traditional way. The passband edge $\theta_a$ and the stopband edge $\varphi_a$ of $H^{(2)}_a(z)$ are easily obtained by [1].
For Case $A$

$$m = \left\lfloor \frac{\omega_p M}{2\pi} \right\rfloor \quad (6a)$$
$$\theta_a = \omega_p M - 2m\pi \quad (6b)$$
$$\varphi_a = \omega_s M - 2m\pi \quad (6c)$$

and for Case $B$

$$m = \left\lceil \frac{\omega_s M}{2\pi} \right\rceil \quad (7a)$$
$$\theta_a = 2m\pi - \omega_s M \quad (7b)$$
$$\varphi_a = 2m\pi - \omega_p M \quad (7c)$$

where $\lfloor x \rfloor$ denotes the largest integer not larger than $x$, and $\lceil x \rceil$ denotes the smallest integer not smaller than $x$. It should be known that both cases must satisfy the condition $0 < \theta_a < \varphi_a < \pi$, and only one case will meet the requirement.

### *A. Determination of the Band Edges of the Masking Filters in the Second Stage*

Let us denote the pass- and stopband edges of $H^{(2)}_{ma}(z)$ and $H^{(2)}_{mc}(z)$ by $\omega^{(2)}_{pma}$, $\omega^{(2)}_{sma}$, $\omega^{(2)}_{pmc}$, and $\omega^{(2)}_{smc}$, respectively. Additionally, the passbands of $H^{(2)}_a(M\omega)$ and its complement ranging from 0 to $\pi$ are numbered as $0, 2, \ldots, 2 \times \lfloor M/2 \rfloor$ and $1, 3, \ldots, 2 \times \lfloor (M-1)/2 \rfloor$, respectively.

*1) Case A:* The magnitude response of the upper branch of $G(z)$ is shown in Fig. 3. Suppose that the passband of $H^{(2)}_a(M\omega)$, marked as $2m$, provides the transition band. Define the "effective passband" as the passband of the masking filter that extracts this transition band. From Fig. 2, we can see that $d_1$ and $d_2$ are the transition bandwidths of the masking filters in the first stage. Therefore, considering the complexity, small $d_1$ and $d_2$ should be avoided. In accordance with Fig. 3, in order to avoid small $d_1$, we set a constraint that at least the passband $2m$ should be extracted completely. In order to avoid small $d_2$, we set a constraint that the passband $2(m+1)$ should be completely outside the effective passband. The two constraints can also be described as follows.

1) The left passband edge of the effective passband, i.e., $x_1$, is no larger than the left stopband edge $\omega_1$ of the passband $2m$.

TABLE I
$\omega_{pma}^{(2)}, \omega_{sma}^{(2)}$ AND THE INEQUALITIES AND VARIABLES FOR $H_{ma}^{(2)}(z)$ IN CASE $A$

| | | |
|---|---|---|
| $Case_p$=$A$ | $\begin{cases}\omega_{pma}^{(2)} = \max(2\pi p - \omega_1 P, \omega_2 P - 2\pi p) \\ \omega_{sma}^{(2)} = \omega_3 P - 2\pi p.\end{cases}$ | (8) |
| $Case_p$=$B$ | $\begin{cases}\omega_{pma}^{(2)} = 2\pi p - \omega_3 P, \\ \omega_{sma}^{(2)} = \min(\omega_1 P - 2\pi(p-1), 2\pi p - \omega_2 P)\end{cases}$ | (9) |
| Inequalities | $x_1 \le \omega_1 = (2\pi m - \varphi_a)/M$ | (10a) |
| | $x_2 \ge \omega_2 = \omega_p$ | (10b) |
| | $x_3 \le \omega_3 = (2\pi(m+1) - \varphi_a)/M$ | (10c) |
| $Case_p$=$A$ | $x_1 = (2\pi p - \omega_{pma}^{(2)})/P$ | (11a) |
| | $x_2 = (2\pi p + \omega_{pma}^{(2)})/P$ | (11b) |
| | $x_3 = (2\pi p + \omega_{sma}^{(2)})/P$ | (11c) |
| $Case_p$=$B$ | $x_1 = (2\pi(p-1) + \omega_{sma}^{(2)})/P$ | (12a) |
| | $x_2 = (2\pi p - \omega_{sma}^{(2)})/P$ | (12b) |
| | $x_3 = (2\pi p - \omega_{pma}^{(2)})/P$ | (12c) |

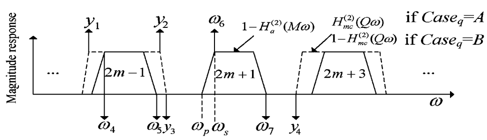


Fig. 4. Magnitude response of the lower branch of $G(z)$.

2) The right passband edge of the effective passband, i.e., $x_2$, is no smaller than the right passband edge $\omega_2$ of the passband $2m$.
3) The right stopband edge of the effective passband, i.e., $x_3$, is no larger than the left stopband edge $\omega_3$ of the passband $2(m+1)$.

The values of $\omega_{pma}^{(2)}, \omega_{sma}^{(2)}$, and the inequalities and variables are shown in Table I, where $p$ is the index of the passbands of $H_{ma}^{(2)}(P\omega)$ satisfying $0 \le p \le \lfloor P/2 \rfloor$. For the given set of $[M, P, Q]$, if there exists $p$ that enables $\omega_{pma}^{(2)}$ and $\omega_{sma}^{(2)}$ to satisfy the three inequalities (10a)–(10c), we continue the design; otherwise, we discard this set of the interpolators. After solving the inequalities (10a)–(10c) by replacing $x_1$, $x_2$, and $x_3$ with (11a)–(11c) when $\text{case}_p = A$ or (12a)–(12c) when $\text{case}_p = B$, we obtained the range of $\omega_{sma}^{(2)}$ and $\omega_{pma}^{(2)}$. Then we take the upper bound of $\omega_{sma}^{(2)}$ and the lower bound of $\omega_{pma}^{(2)}$, respectively, as shown in (8) and (9), such that the transition band of $H_{ma}^{(2)}(z)$ is widest.

It is similar to determining the band edges of $H_{mc}^{(2)}(z)$. The magnitude response of the lower branch of $G(z)$ is shown in Fig. 4. To avoid small $d_1$, passband $(2m-1)$ is kept completely. To avoid small $d_2$, passband $(2m+1)$ is removed completely. $\omega_{pmc}^{(2)}$, $\omega_{smc}^{(2)}$, and the inequalities and variables are shown in Table II, where $q$ is the index of the passbands of $H_{mc}^{(2)}(Q\omega)$ satisfying $0 \le q \le \lfloor Q/2 \rfloor$. After solving the inequalities (14a)–(14d) by replacing $y_1$, $y_2$, $y_3$, and $y_4$ with (15a)–(15d) when $\text{case}_q = A$ or (16a)–(16d) when $\text{case}_q = B$, we obtained the range of $\omega_{smc}^{(2)}$ and $\omega_{pmc}^{(2)}$. Then we take the upper bound of $\omega_{smc}^{(2)}$ and the lower bound of $\omega_{pmc}^{(2)}$, respectively, which are shown in (12d) and (13).

*2) Case B:* The determination of the band edges of $H_{ma}^{(2)}(z)$ is similar to that of $H_{mc}^{(2)}(z)$ in Case $A$. The determination of the band edges of $H_{mc}^{(2)}(z)$ is similar to that of $H_{ma}^{(2)}(z)$ in Case $A$. The values of $(\omega_{pma}^{(2)}, \omega_{sma}^{(2)})$, $(\omega_{pmc}^{(2)}, \omega_{smc}^{(2)})$, and corresponding inequalities and parameters are shown in Tables III and IV, respectively.

TABLE II
$\omega_{pmc}^{(2)}, \omega_{smc}^{(2)}$, AND THE INEQUALITIES AND VARIABLES FOR $H_{mc}^{(2)}(z)$ IN CASE $A$

| | | |
|---|---|---|
| $Case_q$=$A$ | $\begin{cases}\omega_{pmc}^{(2)} = \max(2\pi q - \omega_4 Q, \omega_5 Q - 2\pi q) \\ \omega_{smc}^{(2)} = \min(\omega_6 Q - 2\pi q, 2\pi(q+1) - \omega_7 Q)\end{cases}$ | (12) |
| $Case_q$=$B$ | $\begin{cases}\omega_{pmc}^{(2)} = \max(2\pi q - \omega_6 Q, \omega_7 Q - 2\pi q) \\ \omega_{smc}^{(2)} = \min(\omega_4 Q - 2\pi(q-1), 2\pi q - \omega_5 Q)\end{cases}$ | (13) |
| Inequalities | $y_1 \le \omega_4 = (2\pi(m-1) + \varphi_a)/M$ | (14a) |
| | $y_2 \ge \omega_5 = (2\pi m - \theta_a)/M$ | (14b) |
| | $y_3 \le \omega_6 = \omega_s$ | (14c) |
| | $y_4 \ge \omega_7 = (2\pi(m+1) - \theta_a)/M$ | (14d) |
| $Case_q$=$A$ | $y_1 = (2\pi q - \omega_{pmc}^{(2)})/Q$ | (15a) |
| | $y_2 = (2\pi q + \omega_{pmc}^{(2)})/Q$ | (15b) |
| | $y_3 = (2\pi q + \omega_{smc}^{(2)})/Q$ | (15c) |
| | $y_4 = (2\pi(q+1) - \omega_{smc}^{(2)})/Q$ | (15d) |
| $Case_q$=$B$ | $y_1 = (2\pi(q-1) + \omega_{smc}^{(2)})/Q$ | (16a) |
| | $y_2 = (2\pi q - \omega_{smc}^{(2)})/Q$ | (16b) |
| | $y_3 = (2\pi q - \omega_{pmc}^{(2)})/Q$ | (16c) |
| | $y_4 = (2\pi q + \omega_{pmc}^{(2)})/Q$ | (16d) |

TABLE III
$\omega_{pma}^{(2)}, \omega_{sma}^{(2)}$, AND THE INEQUALITIES AND VARIABLES FOR $H_{ma}^{(2)}(z)$ IN CASE $B$

| | | |
|---|---|---|
| $Case_p$=$A$ | $\begin{cases}\omega_{pma}^{(2)} = \max(2\pi p - P\omega_4, \omega_5 P - 2\pi p) \\ \omega_{sma}^{(2)} = \min(\omega_6 P - 2\pi p, 2\pi(p+1) - \omega_7 P)\end{cases}$ | (17) |
| $Case_p$=$B$ | $\begin{cases}\omega_{pma}^{(2)} = \max(2\pi p - \omega_6 P, \omega_7 P - 2\pi p) \\ \omega_{sma}^{(2)} = \min(\omega_4 P - 2\pi(p-1), 2\pi p - \omega_5 P)\end{cases}$ | (18) |
| Inequalities | $y_1 \le \omega_4 = (2\pi(m-1) - \theta_a)/M$ | (19a) |
| | $y_2 \ge \omega_5 = (2\pi(m-1) + \varphi_a)/M$ | (19b) |
| | $y_3 \le \omega_6 = \omega_s$ | (19c) |
| | $y_4 \ge \omega_7 = (2\pi m + \varphi_a)/M$ | (19d) |
| $Case_p$=$A$ | $y_1 = (2\pi p - \omega_{pma}^{(2)})/P$ | (20a) |
| | $y_2 = (2\pi p + \omega_{pma}^{(2)})/P$ | (20b) |
| | $y_3 = (2\pi p + \omega_{sma}^{(2)})/P$ | (20c) |
| | $y_4 = (2\pi(p+1) - \omega_{sma}^{(2)})/P$ | (20d) |
| $Case_p$=$B$ | $y_1 = (2\pi(p-1) + \omega_{sma}^{(2)})/P$ | (21a) |
| | $y_2 = (2\pi p - \omega_{sma}^{(2)})/P$ | (21b) |
| | $y_3 = (2\pi p - \omega_{pma}^{(2)})/P$ | (21c) |
| | $y_4 = (2\pi p + \omega_{pma}^{(2)})/P$ | (21d) |

TABLE IV
$\omega_{pmc}^{(2)}, \omega_{smc}^{(2)}$, AND THE INEQUALITIES AND VARIABLES FOR $H_{mc}^{(2)}(z)$ IN CASE $B$

| | | |
|---|---|---|
| $Case_q$=$A$ | $\begin{cases}\omega_{pmc}^{(2)} = \max(2\pi q - \omega_1 Q, \omega_2 Q - 2\pi q) \\ \omega_{smc}^{(2)} = \omega_3 Q - 2\pi q.\end{cases}$ | (22) |
| $Case_q$=$B$ | $\begin{cases}\omega_{pmc}^{(2)} = 2\pi q - \omega_3 Q, \\ \omega_{smc}^{(2)} = \min(\omega_1 Q - 2\pi(q-1), 2\pi q - \omega_2 Q)\end{cases}$ | (23) |
| Inequalities | $x_1 \le \omega_1 = (2\pi(m-1) + \theta_a)/M$ | (24a) |
| | $x_2 \ge \omega_2 = \omega_s$ | (24b) |
| | $x_3 \le \omega_3 = (2\pi m + \theta_a)/M$ | (24c) |
| $Case_q$=$A$ | $x_1 = (2\pi q - \omega_{pmc}^{(2)})/Q$ | (25a) |
| | $x_2 = (2\pi q + \omega_{pmc}^{(2)})/Q$ | (25b) |
| | $x_3 = (2\pi q + \omega_{smc}^{(2)})/Q$ | (25c) |
| $Case_q$=$B$ | $x_1 = (2\pi(q-1) + \omega_{smc}^{(2)})/Q$ | (26a) |
| | $x_2 = (2\pi q - \omega_{smc}^{(2)})/Q$ | (26b) |
| | $x_3 = (2\pi q - \omega_{pmc}^{(2)})/Q$ | (26c) |

*B. Determination of the Band Edges of the Masking Filters in the First Stage*

*1) Case A:* For masking filter $H_{ma}^{(1)}(z)$, the passband edge $\omega_{pma}^{(1)}$ is equal to $\omega_p$ since the transition band of $H(z)$ is provided by $H_a^{(2)}(z^M)$. We only need to determine the stopband edge $\omega_{sma}^{(1)}$. Illustration of the determination of $\omega_{sma}^{(1)}$ is shown in Fig. 5.

The stopband edge $\omega_{sma}^{(1)}$ is the right end point of $d_2$, therefore, we pay attention to the first passbands of the masking

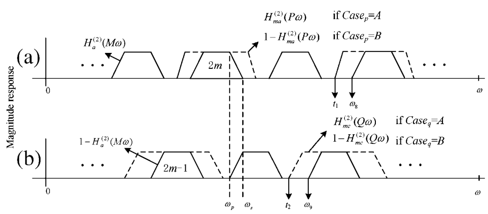


Fig. 5. Process to determine $\omega_{sma}^{(1)}$ for Case $A$.

TABLE V
VALUES OF THE VARIABLES FOR DETERMINING $\omega_{sma}^{(1)}$ IN CASE $A$

| | | |
|---|---|---|
| $Case_p$=A | $t_1 = (2\pi(p+1) - \omega_{sma}^{(2)})/P$ | (32) |
| $Case_p$=B | $t_1 = (2\pi p + \omega_{pma}^{(2)})/P$ | (33) |
| $Case_q$=A | $t_2 = (2\pi(q+1) - \omega_{smc}^{(2)})/Q$ | (34) |
| $Case_q$=B | $t_2 = (2\pi q + \omega_{pmc}^{(2)})/Q$ | (35) |
| | $\omega_8 = (2\pi k_1 - \varphi_a)/M$ | (36) |
| | $\omega_9 = (2\pi k_2 + \theta_a)/M$ | (37) |

filters right to the transition band. The left stopband edges of the two passbands are denoted as $t_1$ and $t_2$, respectively. The position of $t_1$ in $H_a^{(2)}(M\omega)$ and the position of $t_2$ in $1 - H_a^{(2)}(M\omega)$ need to be found out. The pass- and stopband regions of $H_a^{(2)}(M\omega)$ can be calculated as

$$R_{\text{pass}}(k) = \left[\frac{2\pi k - \theta_a}{M}, \frac{2\pi k + \theta_a}{M}\right], \; k = 0, \ldots, \left\lfloor \frac{M}{2} \right\rfloor \tag{27}$$

$$R_{\text{stop}}(k) = \left[\frac{2\pi(k-1) + \varphi_a}{M}, \frac{2\pi k - \varphi_a}{M}\right], k = 0, \ldots, \left\lfloor \frac{M}{2} \right\rfloor \tag{28}$$

where $k$ is the index of the passbands(or stopbands). In accordance with the position of $t_1$, we obtain a temporal value of $\omega_{sma}^{(1)}$, denoted as $\omega_{sma\_\text{temp1}}^{(1)}$

$$\omega_{sma\_\text{temp1}}^{(1)} = \begin{cases} t_1 & t_1 \notin R_{\text{stop}}(k) \\ \omega_8 & t_1 \in R_{\text{stop}}(k_1) \end{cases} \tag{29}$$

where $k_1$ is the index number of the stopband region in which $t_1$ falls into and $\omega_8$ is the right end of $R_{\text{stop}}(k_1)$. In accordance with the position of $t_2$, we obtain a temporal value of $\omega_{sma}^{(1)}$, denoted as $\omega_{sma\_\text{temp2}}^{(1)}$

$$\omega_{sma\_\text{temp2}}^{(1)} = \begin{cases} t_2 & t_2 \notin R_{\text{pass}}(k) \\ \omega_9 & t_2 \in R_{\text{pass}}(k_2) \end{cases} \tag{30}$$

where $k_2$ is the index number of the passband region in which $t_2$ falls into and $\omega_9$ is the right end of $R_{\text{pass}}(k_2)$. The value of $\omega_{sma}^{(1)}$ is obtained by

$$\omega_{sma}^{(1)} = \min\left(\omega_{sma\_\text{temp1}}^{(1)}, \omega_{sma\_\text{temp2}}^{(1)}\right). \tag{31}$$

The values of $t_1$, $t_2$, $\omega_8$ and $\omega_9$ are listed in Table V.

For masking filter $H_{mc}^{(1)}(z)$, the stopband edge $\omega_{smc}^{(1)}$ equals to $\omega_s$, and we only need to determine the passband edge $\omega_{pmc}^{(1)}$. Illustration of the determination of $\omega_{pmc}^{(1)}$ is shown in Fig. 6. Since $\omega_{pmc}^{(1)}$ is the left endpoint of $d_1$, for $H_{ma}^{(2)}(P\omega)$, we pay attention to the passband that contains the transition band. For $H_{mc}^{(2)}(Q\omega)$, we pay attention to the first passband left to the transition band. The left passband edges of these two passbands are denoted as $t_3$ and $t_4$, respectively.

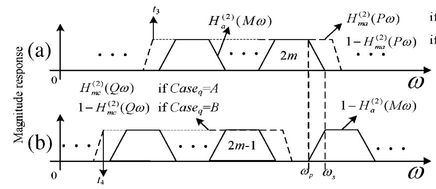


Fig. 6. Process to determine $\omega_{smc}^{(1)}$ for Case $A$.

TABLE VI
VALUES OF THE VARIABLES FOR DETERMINING $\omega_{pmc}^{(1)}$ IN CASE $A$

| | | |
|---|---|---|
| $Case_p$=A | $t_3 = (2\pi p - \omega_{pma}^{(2)})/P$ | (40) |
| $Case_p$=B | $t_3 = (2\pi(p-1) + \omega_{sma}^{(2)})/P$ | (41) |
| $Case_q$=A | $t_4 = (2\pi q - \omega_{pmc}^{(2)})/Q$ | (42) |
| $Case_q$=B | $t_4 = (2\pi(q-1) + \omega_{smc}^{(2)})/Q$ | (43) |

If $t_3 \geq t_4$, we have

$$\omega_{pmc}^{(1)} = \begin{cases} t_3 & t_3 \notin R_{\text{stop}}(k) \\ \max\left((2\pi(k_3-1) + \varphi_a)/M, t_4\right) & t_3 \in R_{\text{stop}}(k_3). \end{cases} \tag{38}$$

If $t_3 < t_4$, we have

$$\omega_{pmc}^{(1)} = \begin{cases} t_4, & t_4 \notin R_{\text{pass}}(k) \\ \max\left((2\pi k_4 - \theta_a)/M, t_3\right), & t_4 \in R_{\text{pass}}(k_4). \end{cases} \tag{39}$$

$k_3$ is the index number of the stopband region in which $t_3$ falls into, and $k_4$ is the index number of the passband region in which $t_4$ falls into. The values of $t_3$ and $t_4$ are listed in Table VI.

*2) Case B:* The determinations of $\omega_{sma}^{(1)}$ and $\omega_{pmc}^{(1)}$ in Case $B$ are similar with that in Case $A$, and the parameters are shown in Tables VII and VIII, respectively. It should be pointed out that all the band edges of subfilters must range from 0 to $\pi$; otherwise, the set of $[M, P, Q]$ is invalid for the further design procedures.

## III. DESIGN EXAMPLES AND ANALYSIS

The process of finding the best $[M, P, Q]$ can be described as follows,

1) Search through all the combinations of $[M, P, Q]$. For each set, estimate the number of multipliers needed for the two-stage FRM based on the set.
2) There exists a set of $[M, P, Q]$ for which the estimated number of multipliers is smallest. In accordance with the suggestion in [8], the candidates with the number of multipliers less than 105% of the smallest number are also taken into consideration for further optimization.
3) For each set of $[M, P, Q]$, the subfilters are produced and optimized using nonlinear optimization in [8].
4) Among all the sets that lead to the final filters that meet the specifications, the one with the minimum number of multipliers is chosen as the solution. If there are two or more solutions, the one with the shortest group delay is chosen.

*Example 1:* Example 1 is a narrow transition-band filter with specifications $\omega_p = 0.6\pi$, $\omega_s = 0.602\pi$, $\delta_p = 0.01$, and $\delta_s = 40$ dB. With the proposed method, the best solution is obtained with $N_a = 28$, $N_{ma2} = 20$, $N_{mc2} = 16$, $N_{ma} = 17$, and $N_{mc} = 29$. The interpolation factors $M$, $P$, and $Q$ are 69, 9, and 9, respectively. It is a Case $B$ design with $\text{Case}_p = B$ and $\text{Case}_q = B$. The number of multipliers is 59, and the group

TABLE VII
VALUES OF THE VARIABLES FOR DETERMINING $\omega_{sma}^{(1)}$ IN CASE $B$

| | | |
|---|---|---|
| $Case_p$=A | $t_2 = \left(2\pi(p+1) - \omega_{sma}^{(2)}\right)/P$ | (44) |
| $Case_p$=B | $t_2 = (2\pi p + \omega_{pma}^{(2)})/P$ | (45) |
| $Case_q$=A | $t_1 = (2\pi(q+1) - \omega_{smc}^{(2)})/Q$ | (46) |
| $Case_q$=B | $t_1 = (2\pi q + \omega_{pmc}^{(2)})/Q$ | (47) |
| | $\omega_8 = (2\pi k_1 + \theta_a)/M$ | (48) |
| | $\omega_9 = (2\pi k_2 - \varphi_a)/M$ | (49) |

TABLE VIII
VALUES OF THE VARIABLES FOR DETERMINING $\omega_{pmc}^{(1)}$ IN CASE $B$

| | | |
|---|---|---|
| $Case_p$=A | $t_4 = \left(2\pi p - \omega_{pma}^{(2)}\right)/P$ | (50) |
| $Case_p$=B | $t_4 = (2\pi(p-1) + \omega_{sma}^{(2)})/P$ | (51) |
| $Case_q$=A | $t_3 = (2\pi q - \omega_{pmc}^{(2)})/Q$ | (52) |
| $Case_q$=B | $t_3 = (2\pi(q-1) + \omega_{smc}^{(2)})/Q$ | (53) |

TABLE IX
DESIGN RESULTS AND COMPARISONS FOR EXAMPLE 1

| Methods | $N_{mult}$ | Group Delay |
|---|---|---|
| Conventional two-stage FRM [10] | 92 | 1105 |
| Overall optimization FRM[ 8] | 62 | 1067 |
| Non-periodical FRM [9] | 55 | 1214 |
| Proposed | 59 | 1070.5 |

delay is 1070.5. The passband ripple and the stopband attenuation ripple are 0.010 and 40.0109 dB, respectively. Comparisons with several other two-stage designs are shown in Table IX, where $N_{\text{mult}}$ is the number of multipliers in the overall system.

Compared with the conventional two-stage FRM [10], the number of multipliers is reduced by 35.8%, and the group delay is reduced by 3.1%. Compared with the nonperiodical FRM [9], the number of multipliers is increased by 7.3%, whereas the group delay is reduced by 11.8%. The difference above may be caused by the different optimization methods used. Therefore, it is meaningful to compare our work with [8], which uses the same optimization method. Compared with [8], the number of multipliers is reduced by 4.8%, whereas the group delay is increased by 0.3%.

*Example 2:* The filter of example 2 has a larger transition band than the filter of example 1 with passband edge $\omega_p = 0.6$, stopband edge $\omega_s = 0.61\pi$, passband ripple $\delta_p = 0.003643$, and stopband ripple $\delta_s = 48.78$ dB. Using the proposed method, the optimal interpolation factors are $M = 19$, $P = 4$, and $Q = 4$. It is a Case $B$ design with $\text{Case}_p = A$ and $\text{Case}_q = A$. The orders of subfilters $H_a^{(2)}(z)$, $H_{ma}^{(2)}(z)$, $H_{mc}^{(2)}(z)$, $H_{ma}^{(1)}(z)$, and $H_{mc}^{(1)}(z)$ are 26, 10, 16, 11, and 15, respectively. The maximum ripple in the passband is 0.0033, and the attenuation in the stopband is 49.5651 dB. The results compared with other work are listed in Table X. The complexity in terms of number of multipliers of the proposed method is lowest among the methods in the table. Compared with [8], which uses the same optimization algorithm, the number of multipliers is reduced by 2.3%, and the group delay is also reduced by 1.5% for design 1 and 7.6% for design 2.

It is necessary to have a further look at the comparison with the work in [9], which is our previous work, and the work in [8], which represents the state of the art of the two-stage FRM. In [9], by using the same prototype filter to generate all the subfilters at the second stage (we can regard it as using the single filter frequency masking method), the structure in [9] may achieve smaller complexity compared with that of the proposed structure. However, in the examples, the complexity of the proposed structure is smaller than that of [9]. This reduction of complexity may come from the usage of joint optimization.

TABLE X
DESIGN RESULTS AND COMPARISONS FOR EXAMPLE 2

| Ref | $N_a$ | $N_{ma2}$ | $N_{mc2}$ | $N_{ma}$ | $N_{mc}$ | $N_{mult}$ | Group delay |
|---|---|---|---|---|---|---|---|
| [3] | 26 | 12 | 26 | 14 | 22 | 55 | 271 |
| [6] | 26 | 10 | 22 | 12 | 20 | 50 | 262 |
| [5] | 32 | 8 | 14 | 10 | 14 | 44 | 291 |
| [8](design1) | 32 | 8 | 14 | 10 | 14 | 44 | 291 |
| [8](design2) | 22 | 20 | 14 | 10 | 12 | 44 | 310 |
| [9] | 30 | --- | --- | 25 | 29 | 44 | 240 |
| Proposed | 26 | 10 | 16 | 11 | 15 | 43 | 286.5 |

Since we adopted the optimization approach proposed in [8], the comparison with [8] is fair. Sometimes, the solution of the proposed method may be the same as that of [8], which means it happened that the conventional design could find the optimal solution. For example, when using the proposed method to design a low-pass filter with the band edges at (0.2, 0.201), passband ripple of 0.01, and stopband attenuation of $-60$ dB, the optimal interpolation factors are $M = 54$, $P = 9$, and $Q = 9$ [$M$, $P$, and $Q$ satisfy (3)]. For other examples in this brief, the set of the interpolation factors obtained by the proposed method is different with that of [8], which are more efficient designs whose efficiency comes from the modification of the structure. In fact, removing the constraints on the interpolation factors enables us to search the solution in a wider space. Some cases that are excluded due to the constraints on the conventional structure are now included in our consideration. Thus, the proposed structure results in the possibility of improvement, in complexity and/or delay.

## REFERENCES


[1] Y. C. Lim, "Frequency-response masking approach for the synthesis of sharp linear phase digital filters," *IEEE Trans. Circuits Syst.*, vol. CAS-33, pp. 357–364, Apr. 1986.

[2] Y. C. Lim and Y. Lian, "The optimum design of one- and two-dimensional FIR filters using the frequency response masking technique," *IEEE Trans. Circuits Syst. II, Analog Digit. Signal Process.*, vol. 40, no. 2, pp. 88–95, Feb. 1993.

[3] W.-S. Lu and T. Hinamoto, "Optimal design of frequency-response-masking filters using semidefinite programming," *IEEE Trans. Circuits Syst. I*, vol. 50, no. 4, pp. 557–568, Apr. 2003.

[4] Y. J. Yu, T. Saramäki, and Y. C. Lim, "An iterative method for optimizing FIR filters synthesized using the two-stage frequency-response masking technique," in *Proc. IEEE Int. Symp. Circuits Syst.*, Bangkok, Thailand, May 25–28, 2003, pp. III-874–III-877.

[5] W. R. Lee, L. Caccetta, K. L. Teo, and V. Rehbock, "A unified approach to multistage frequency-response masking filter design using the WLS technique," *IEEE Trans. Signal Process.*, vol. 54, no. 9, pp. 3459–3467, Sep. 2006.

[6] X.-H. Wang and Y.-G. He, "A neural network approach to FIR filter design using frequency-response masking technique," *Signal Process.*, vol. 88, no. 12, pp. 2917–2926, Dec. 2008.

[7] J. Yli-Kaakinen, T. Saramaki, and Y. J. Yu, "An efficient algorithm for the optimization of FIR filters synthesized using the multistage frequency-response masking approach," in *Proc. Int. Symp. Circuits Syst.*, vol. 5, pp. 540–543, May 2004.

[8] J. Yli-Kaakinen and T. Saramaki, "An efficient algorithm for the optimization of FIR filters synthesized using the multistage frequency-response masking approach," *Circuits Syst. Signal Process.*, vol. 30, no. 1, pp. 157–183, Feb. 2011.

[9] Y. Wei and D. Liu, "Improved design of frequency-response masking filters using band-edge shaping filter with non-periodical frequency response," *IEEE Trans. Signal Process.*, vol. 61, no. 13, Jul. 1, 2013.

[10] Y. C. Lim and Y. Lian, "The optimal design of one- and two- dimensional FIR filters using the frequency response masking technique," *IEEE Trans. Circuits Syst. II*, vol. 40, no. 2, pp. 88–95, Feb. 1993.